Nature Communications

https://doi.org/10.1038/s41467-026-69429-6

Article in Press

Sequencing DNA methylation and hydroxymethylation at co-occurring chromatin features

Received: 17 June 2025

Accepted: 2 February 2026

Cite this article as: Araujo Tavares, R.d., Dhir, S., He, X. *et al.* Sequencing DNA methylation and hydroxymethylation at co-occurring chromatin features. *Nat Commun* (2026). https://doi.org/10.1038/s41467-026-69429-6

Rafael de Cesaris Araujo Tavares, Somdutta Dhir, Xuan He, Jack Monahan, Minna Taipale, Paula Golder, Aldo Ciau-Uitz, Walraj Gosal, David Tannahill & Shankar Balasubramanian

Sequencing DNA methylation and hydroxymethylation at co-occurring chromatin features

Rafael de Cesaris Araujo Tavares[1], Somdutta Dhir[1], Xuan He[2], Jack Monahan[3], Minna Taipale[3], Paula Golder[3], Aldo Ciau-Uitz[3], Walraj Gosal[3], David Tannahill[1] & Shankar Balasubramanian[1,2,4,*]

[1] Cancer Research UK Cambridge Institute, Li Ka Shing Centre, Robinson Way, Cambridge, CB2 0RE, UK
[2] Yusuf Hamied Department of Chemistry, University of Cambridge, Cambridge, CB2 1EW, UK
[3] biomodal, The Trinity Building, Chesterford Research Park, CB10 1TS, UK
[4] School of Clinical Medicine, University of Cambridge, Cambridge, CB2 0SP, UK
** Correspondence: sb10031@cam.ac.uk (S.B.)*

Abstract

Epigenetic modifications govern chromatin dynamics and cell state. However, current methods cannot simultaneously resolve the presence of multiple DNA modifications at co-occurring chromatin-associated features. It is thus not clear how these features are physically coupled and how their combinations regulate genome function. To address this key question, we report 6-base-CUT&Tag, a method for simultaneous 6-base sequencing at target chromatin features. Using 6-base-CUT&Tag to profile 5-methylcytosine (5mC) and 5-hydroxymethylcytosine (5hmC) at co-occurring histone modifications in mouse embryonic stem cells, we identify feature-dependent 5mC/5hmC signatures previously unresolvable with untargeted or bisulfite-based workflows. We show that DNA methylation and hydroxymethylation are specifically coupled with the H3K4me1 mark in mESC enhancers and that H3K4me1-derived signatures robustly distinguish different enhancer functional states.

Introduction

Chemical modifications of DNA bases and histone tails regulate physical and functional properties of chromatin, including DNA accessibility, genomic architecture and binding of transcription regulators[1-4]. Methylation of cytosine bases on DNA is critical to establish the epigenetic landscape and governs gene activity and inheritance[5]. Cytosine bases can be methylated by DNA methyltransferases (DNMTs), that transfer a methyl group from the donor S-adenosylmethionine to form 5-methylcytosine (5mC)[6], which can be further oxidised to form 5-hydroxymethylcytosine (5hmC) through the action of the Ten-Eleven Translocation family of proteins (TETs 1-3)[7]. TET enzymes can further oxidise 5hmC to other intermediates like 5-formylcytosine (5fC) and 5-carboxylcytosine (5caC)[8], each of which can be excised by thymine DNA glycosylase, followed by restoration of C, completing a demethylation cycle (Figure 1a). 5mC is the most abundant cytosine modification (2-4% of all Cs in ESCs) and 5hmC is the next most abundant cytosine modification (0.1-0.2% of all Cs in ESCs), with 5fC and 5caC being present at substantially lower levels (~0.002% and ~0.0003%, respectively)[8]. While 5hmC can be an intermediate in active DNA demethylation, it has also been shown to be a stable epigenetic mark that is associated with transcriptional activity and cell fate[9-14]. The functional roles of 5mC and 5hmC depend on their genomic context. Broadly, 5mC enrichment at promoters and enhancers is associated with transcriptional repression[15,16], whereas 5hmC is enriched at active regulatory regions – particularly enhancers – and also within the gene bodies of transcriptionally active genes[17,18].

The development of sequencing methods to detect 5mC and 5hmC has been an important focus in epigenomics. While early methods such as bisulfite sequencing[19] cannot distinguish 5hmC from 5mC, later approaches – including oxidative bisulfite sequencing[20], TET-assisted bisulfite sequencing[21], APOBEC-coupled epigenetic sequencing[22], pyridine borane sequencing

methods[23,24] and third-generation sequencing platforms (e.g., PacBio, Oxford Nanopore)[25] – have enabled base-resolution mapping of both 5mC and 5hmC. More recent methods have now leveraged state-of-the-art enzymology and chemistry to enable bisulfite-free and simultaneous detection of 5mC and 5hmC on the same DNA fragment[26-28].

Despite such advancements, a key challenge in the field has been to determine how 5mC and 5hmC are coupled in space and time to other chromatin features such as histone marks, transcription factors and chromatin remodelers. Establishing this relationship is critical to appreciate how epigenetic features are coupled, when and where they co-occur, and how they determine causal relationships and regulatory roles. Current strategies that map DNA modifications and chromatin features largely rely on comparing profiling data from independent experiments for different features. This approach does not necessarily determine co-occurrence of features at the molecular level (Figure 1b). Earlier attempts to address this limitation have coupled ChIP-seq and CUT&Tag with bisulfite sequencing to determine cytosine methylation on DNA fragments directly associated with chromatin proteins[29-32]. However, these methods have major limitations that include substantial loss of DNA caused by bisulfite-mediated degradation[33], which precludes analysis of smaller sample quantities. Crucially, the inability to discriminate between C, 5mC and 5hmC bases at read level in the same workflow[34] is a major gap in our understanding of how combinations of epigenetic features influence genome regulation.

Here, we introduce 6-base-CUT&Tag sequencing (abbreviated 6B-C&T), a method to simultaneously map G, A, T, C, 5mC and 5hmC bases at co-occurring chromatin-associated features. 6B-C&T begins with targeted antibody enrichment of specific chromatin features via CUT&Tag that are purified from a heterogeneous pool, followed by an updated 6-base library preparation workflow, sequencing and analysis (Figure 1c). This approach substantially reduces sequencing depth requirements and cost relative to whole-genome sequence analysis (see Methods, Supplementary Data 1). We demonstrate that 6B-C&T reveals hidden 5mC/5hmC signatures which are feature-dependent and have not been recoverable in previous untargeted or bisulfite-based workflows.

Results

6-base-CUT&Tag (6B-C&T) development

As proof-of-concept for 6-base-CUT&Tag (6B-C&T), we used E14TG2A mouse embryonic stem cells (mESCs) and initially chose H3K27ac, a highly prevalent histone mark in active chromatin, as the feature to profile (Figure 1c). Using an antibody selective for H3K27ac, we first performed antibody-directed pA-Tn5 tagmentation with a uracil-containing hairpin mosaic-end adaptor, termed ME2U. Tagmented DNA is then subjected to circularisation to generate dumbbell-like molecules that are resistant to exonuclease treatment. Uracil-specific excision reagent (USER) treatment digests the uracil sites of the adaptor, allowing the strands to separate and the residual hairpin sequences on each strand to refold independently. This produces DNA suitable for our 6-base-seq enzymatic conversion workflow[26] (Figure 1c, Supplementary Figure 1). After Illumina paired-end sequencing, the four canonical DNA bases and two cytosine epigenetic states can be resolved on individual reads to provide the G, A, T, C, 5mC and 5hmC sequence context at H3K27ac sites.

An important element in the development of 6B-C&T was to avoid interference from partially tagmented or randomly cleaved DNA, which would be a major source of non-specific background. To address this, we took advantage of the ‘scar’ sequences left on both strands of the DNA fragment after USER digestion of the inserted ME2U hairpin. These residual sequences are

copied and deaminated prior to PCR amplification (Figure 2a) and thus serve as an internal benchmark to identify valid read pairs derived from double-sided hairpin constructs. Furthermore, circularisation of double-sided hairpin constructs makes them resistant to exonuclease digestion, as opposed to non-specifically cleaved or partially tagmented DNA. Motivated by related strategies to remove similar DNA fragments [35,36], we determined that a mixture of T7 Exonuclease (dsDNA-specific), RecJf and Exonuclease I (ssDNA-specific) achieved the highest recovery of scarred read pairs relative to a protocol with no enzyme treatment or with other enzyme combinations (Figure 2a).

In our initial H3K27ac 6B-C&T in mESCs, scar-filtered read pairs mapped to regions that strongly overlapped with H3K27ac sites determined independently using standard CUT&Tag (Figure 2b-c; Supplementary Figures 2-3). To verify the accuracy of DNA modification measurement, we included three different synthetic spike-ins as fiducials (Methods) that were also subjected to 6-base-seq base conversions alongside tagmented mESC DNA. For each DNA control (5mC-modified Lambda DNA, 5hmC-modified oligonucleotide and unmodified pUC19 DNA), we achieved high sensitivity (98-99.5%) in identifying the true cytosine modification state (Figure 2d). These results show that 6B-C&T can faithfully recapitulate the genomic distribution of a target feature and simultaneously detect 5mC and 5hmC bases with high accuracy.

Having validated 6B-C&T on H3K27ac, we set out to profile 5mC and 5hmC in mESCs at each of several histone modifications marking distinct types of regulatory elements[37]. For this, we included H3K27ac (active enhancers and promoters), H3K4me3 (promoters), H3K4me1 (enhancers) and H3K27me3 (Polycomb-repressed, bivalent chromatin), along with a non-specific IgG control. As a reference, we also performed whole-genome 6-base-seq, which provides an untargeted picture representative of the total pool of DNA fragments. Using this approach, we confirmed that the global relative 5mC/5hmC abundance on genomic DNA was consistent with reported values in mESCs (Supplementary Figure 4a). Genomic enrichments obtained by 6B-C&T were highly reproducible across experimental replicates for each histone mark (Pearson $r \geq 0.97$) and showed good agreement (Pearson $r \geq 0.86$) when compared to standard CUT&Tag (Supplementary Figure 5). CpG modification levels (i.e. the fraction of CpGs detected as 5mC or 5hmC) at each histone mark also showed excellent reproducibility (Pearson $r \geq 0.90$, Supplementary Figure 6). Finally, we assessed how well 6B-C&T correlates with CUT&Tag-BS, a method that profiles total cytosine methylation (modC) on CUT&Tag DNA fragments via bisulfite conversion[32]. Both genomic feature enrichment and CpG modification levels for 6B-C&T agreed well with publicly available CUT&Tag-BS data for H3K4me1 and H3K27me3 (Pearson $r \geq 0.83$, Supplementary Figure 7).

Measuring 5mC and 5hmC at distinct histone modifications

Methylation is known to be depleted in histone mark-enriched regulatory regions relative to the other regions in the mESC genome[38]. Consistent with this, we observed that average 5mC and 5hmC levels in 6B-C&T were lower than in the whole-genome (untargeted) 6-base-seq experiment (Supplementary Figure 4a). This difference is due to the 6B-C&T method specifically capturing DNA fragments at histone mark-enriched sites, which are generally less (hydroxy)methylated compared to the whole genome. Furthermore, when looking at individual histone marks, we found that those associated with active chromatin (H3K4me3, H3K27ac, H3K4me1) showed lower overall methylation and a higher 5hmC/5mC ratio than the bivalent/repressed chromatin (H3K27me3) mark, a pattern that was absent in whole-genome data (Supplementary Figure 4b, Supplementary Figure 8). Globally, individual CpG sites captured by 6B-C&T mapped to regions with high histone mark enrichment and showed differences in 5mC and 5hmC levels relative to the untargeted method (Supplementary Figure 9).

We next investigated how 5mC and 5hmC levels in 6B-C&T differed from untargeted 6-base-seq data for the same CpG sites (Supplementary Figure 10a). First, we identified CpG sites with statistically significant differences between both methods, i.e., differentially methylated CpGs (DMCs) and differentially hydroxymethylated CpGs (DHMCs). While most DHMCs between both methods were located in introns followed by intergenic and promoter regions, DMCs were primarily found in promoters followed by introns/exons (Supplementary Figure 10b-e). Overall, DMCs predominantly showed lower 5mC levels in 6B-C&T relative to whole-genome (untargeted) data (Supplementary Figure 10a, Supplementary Figure 11). This suggests that DNA associated with histone modifications at these sites is mostly hypomethylated relative to the total pool of DNA fragments. This was particularly striking in DMCs co-occurring with H3K4me3 at imprinted gene loci[39] such as *Igfr2*, *Kcnq1ot1* and *Peg3*, suggesting that this active histone mark largely associates with the unmethylated allele (Supplementary Figure 10a). For DHMCs, active chromatin marks (H3K4me3, H3K27ac and H3K4me1) showed similar numbers of sites with higher or lower 5hmC levels in 6B-C&T relative to the untargeted experiment; in contrast, for the repressive mark (H3K27me3) the majority of DHMCs showed higher 5hmC levels in 6B-C&T than in untargeted 6-base-seq (Supplementary Figure 10a, Supplementary Figure 11). Overall, these observations reveal important epigenetic differences between the DNA associated with target histone modifications and the bulk average at the same genomic sites. These quantitative relationships would be difficult to discern from comparative analysis of independent measurements of 5mC, 5hmC and histone marks.

Histone mark-specific 5mC and 5hmC enrichments at enhancers

To demonstrate the applicability of 6B-C&T to determine the true base modification status at specific chromatin elements, we analysed a set of mESC enhancers that have been independently annotated by the presence or absence of specific histone marks by ChIP-seq[40], including active (H3K27ac, H3K4me1), primed (H3K4me1) and poised (H3K4me1, H3K27me3) enhancers. We observed good agreement at these loci between 6B-C&T and the ChIP-seq data originally used for their annotation (Supplementary Figure 12). Excellent agreement was also obtained for total DNA methylation levels (%modC) at all enhancer types between 6B-C&T and available C&T-BS data for the general enhancer mark, H3K4me1 (Supplementary Figure 7c). We next found that different enhancer loci displayed distinct patterns of 5mC and 5hmC enrichment (Figure 3a, Supplementary Figure 13). Across all enhancer types, primed enhancers, defined by H3K4me1 alone, generally showed the highest levels of both 5mC (average ~13%) and 5hmC (average ~4%; Figure 3b). It is notable that this increased enrichment at the H3K4me1 mark was specific to primed enhancers, since other H3K4me1-associated CpG sites showed much lower 5mC and 5hmC levels (Supplementary Figure 14; Supplementary Data 1 – Table 1). In contrast, active and poised enhancers were relatively depleted of both 5mC (~4% for active and ~2% for poised, on average) and 5hmC (~2% for active and poised, on average). For all enhancer types, H3K4me1 consistently showed the highest 5mC and 5hmC levels and the highest 5mC/5hmC ratio among all histone marks (Figure 3b).

We then assessed whether the enrichment of 5mC and 5hmC at primed enhancers was specific to H3K4me1 by measuring these DNA modifications at other enhancer-associated histone marks potentially present at these sites i.e., H3K27ac and H3K27me3. We first confirmed that annotated primed enhancers were enriched with the H3K4me1 mark but also showed appreciable levels of H3K27ac and H3K27me3 (Figure 3c, Supplementary Figure 15). Across all three histone marks, H3K4me1 displayed the highest fraction of both 5mC and 5hmC, and the highest 5mC/5hmC ratio (Figure 3d, Supplementary Figure 16). This pattern, which cannot be detected with previously reported methods like ChIP-BS[41], suggests that H3K4me1-marked nucleosomes are sites for

preferential 5mC retention at enhancers. Active (H3K27ac) and bivalent (H3K27me3) histone marks, which do not represent the primed enhancer state, showed a greater tendency towards demethylation (lower overall methylation levels, higher 5hmC/5mC ratio). These results suggest that 5mC and 5hmC are coupled to different extents with each chromatin mark and, more generally, that different enhancer states are defined by distinct combinations of epigenetic modifications.

5mC and 5hmC at H3K4me1 resolves distinct enhancer functional states

H3K4me1 is common to all enhancer functional states, so we next asked whether 6B-C&T methylation at this single feature better resolves different enhancer types compared to the more heterogenous whole genome (untargeted) 6-base-seq data. For this, we used H3K4me1 6B-C&T data to train a machine learning model for classification of enhancer types (active, primed and poised) and compared its performance to a model with the same architecture trained on whole-genome 6B-seq data (Figure 4a, Supplementary Figure 17). For all enhancer types, the 6B-C&T-derived model showed superior performance when compared to the whole genome-derived model (Figure 4b-d; Supplementary Figure 18). This demonstrates that the H3K4me1-coupled 5mC and 5hmC signal more robustly resolves *bona fide* enhancer states than its unenriched equivalent. These results show that 6B-C&T can be used to evaluate co-occurring epigenetic features and retrieve improved information on individual molecular states (Figure 1b).

Discussion

6B-C&T detects 5mC and 5hmC bases that co-occur with target chromatin features. Profiling of major regulatory histone modifications, such as H3K4me1 and H3K27me3, reveals patterns that are consistent with other measurements of total DNA methylation at these marks[32,41,42] and adds 5hmC as a new dimension to the multiomics analysis of individual DNA fragments. Interrogation of feature-specific 5mC/5hmC signatures provides a higher-resolution framework for mechanistic dissection of methylation dynamics at transcriptional regulatory elements.

To exemplify the utility of 6B-C&T we used it to dissect the epigenetic heterogeneity of mESC enhancers and found that the accumulation of 5mC and 5hmC in these regions depends on the associated histone mark. Furthermore, although all enhancer functional states are marked by H3K4me1, the co-occurrence of 5mC and 5hmC on the same DNA fragment with this histone modification had never been measured. Here, we show that both DNA marks co-occur at significantly higher levels with H3K4me1 than with other histone marks. Our machine learning analysis shows how these different layers of epigenetic information (i.e., histone and DNA modifications) are coupled and intrinsically linked with enhancer functional states. Importantly, the use of H3K4me1-specific methylation signatures enables the identification of functional enhancer states without the need for whole-genome sequencing or multiple histone mark enrichment profiles.

Our work allows for the precise measurement of coupled epigenetic features at individual loci and has the potential to largely expand the combinatorial epigenetic code. Discriminating at read level between multiple combinations of epigenetic marks will be paramount to dissect their inherently different functional roles and mechanisms. Our method also has the practical advantage of lower sequencing depth and cost, as compared to multiple whole-genome sequencing runs. We envisage routine application of 6B-C&T will provide new insights into how different epigenetic layers combine to modulate chromatin behaviour and cellular phenotype.

Methods

Cell culture

E14TG2A mouse embryonic stem cells were cultured in serum/LIF conditions on gelatin-coated plates. Serum/LIF medium was prepared with high-glucose DMEM (Sigma, D6546-500mL) supplemented with 10% FBS (Gibco, 16141079), 1X GlutaMax-I (Gibco, 35050-038), 1X NEAA (Gibco, 11140-035), 0.1 mM β-mercaptoethanol (Sigma, M3148) and 1,000 U/mL LIF (PeproTech, murine LIF, 250-02-25UG). For maintenance, cells were grown until 70-80% confluent and sub-cultured by dissociation with StemPro Accutase Cell Dissociation Reagent (Invitrogen A1110501). Cultures were routinely monitored and tested negative for Mycoplasma contamination. E14TG2A cells were a gift from Wolf Reik (Babraham Institute, Cambridge).

Preparation of tagmentation adaptors

Tn5ME-A, Tn5ME-B and Tn5MErev oligonucleotides were reconstituted to 200 µM in annealing buffer (10 mM Tris-HCl pH 8.0, 50 mM NaCl, 1 mM EDTA). Tn5ME-A and Tn5ME-B were mixed separately with equal amounts of Tn5MErev and annealed on a thermocycler (95°C for 2 min, then cooled in 5°C steps with 5 min incubation at each step until 25°C). The resulting mosaic-end adaptors are termed MEDS-A and MEDS-B, respectively. The ME2U hairpin adaptor was reconstituted to 25 µM in Nuclease-Free Duplex Buffer (30 mM HEPES, pH 7.5; 100 mM potassium acetate, IDT11-01-03-01) and annealed by heat denaturation at 95°C for 2 min, followed by slow cooling at 0.1°C/second to 10°C. All oligonucleotide sequences (including chemical modifications) are listed in Supplementary Data 1 (Table 2).

pA-Tn5 transposome assembly

pA-Tn5 transposase was prepared in-house[43] or obtained commercially (Active Motif, 53162) and loaded with application-specific DNA adaptors. For the standard CUT&Tag workflow, 50 µL of pA-Tn5 (4 µM) were mixed with a 3-fold excess of each pre-annealed mosaic-end adaptor, MEDS-A and MEDS-B, and rotated at room temperature for 1 hour. For 6-base-CUT&Tag, 50 µL of pA-Tn5 (4 µM) were mixed with a 3-fold excess of folded ME2U hairpin adaptor and similarly rotated at room temperature for 1 hour. Transposome samples were stored at -20°C.

Standard CUT&Tag (Cleavage Under Targets and Tagmentation)

Standard CUT&Tag was performed as in Kaya-Okur et al.[44] with modifications. Briefly, *Dynabeads MyOne Streptavidin T1* beads (Invitrogen 65601) were conjugated with biotinylated ConA[45] (Sigma C2272) and activated in binding buffer (20 mM HEPES pH 7.5, 10 mM KCl, 1 mM $CaCl_2$, 1 mM $MnCl_2$) prior to cell binding. 500,000 cells per assay were lightly fixed for 2 min with 0.1%

formaldehyde in PBS and fixation was stopped by adding glycine to a final concentration of120 mM. Fixed cells were resuspended in wash buffer (20 mM HEPES pH 7.5, 150 mM KCl, 0.5 mM spermidine and Complete EDTA-Free Protease Inhibitor, Roche 11873580001) and immediately bound to ConA-conjugated *MyOne T1* beads. Primary antibody binding was performed overnight at 4°C in wash buffer supplemented with 0.05% digitonin (Sigma 300410-250MG), 2 mM EDTA, 0.1% BSA and 1:50 dilutions of antibody stocks (H3K27ac – Abcam, ab4729-100ug; H3K4me1 – Abcam, ab8895; H3K4me3 – Abcam, ab8580; H3K27me3 – Cell Signaling Technology, 9733; normal rabbit IgG – Cell Signaling Technology, 2729). For secondary antibody binding, a guinea pig anti-rabbit IgG (Antibodies-Online ABIN101961:2 µg) was diluted 1:25 in dig-wash buffer (wash buffer + 0.05% digitonin) and binding performed at 25°C for one hour. pA-Tn5-MEDS-A/B transposome was diluted 1:250 in dig-300 buffer (20 mM HEPES pH 7.5, 300 mM KCl, 0.5 mM spermidine, 0.01 % digitonin and Complete EDTA-Free Protease Inhibitor) and allowed to bind at 25°C for one hour. Feature-specific tagmentation was done in dig-300 buffer supplemented with 10 mM $MgCl_2$ at 37°C for one hour and stopped by washing cells with TAPS wash buffer (10 mM TAPS pH 8.5, ThermoScientific J63268.AE + 0.2 mM EDTA). DNA was released and cross links were reversed by Proteinase K treatment at 55°C for one hour (0.5 mg/mL Proteinase K Invitrogen EO0491, 0.5% SDS, 10 mM Tris-HCl pH 8.0), followed by clean-up with Zymo DNA Clean and Concentrator (Zymo Research D4013). PCR was carried out using Q5 Hot Start High-Fidelity 2X Master Mix (M0494S) and indexed primers (Supplementary Data 1 – Table 2) on a thermocycler (program: 72°C for 5 min, 98°C 30s; 12 cycles of 98°C 10s, 63°C 10s; final extension at 72°C 1 min; 4°C hold). PCR products were purified by double-sided size selection with AMPure XP beads (Beckman Coulter A63880, 0.4X followed by 1.3X). QC was performed on a 4200 TapeStation (Agilent) and libraries were quantified using the NEBNext library quantification kit (E7630L). Libraries were sequenced on Illumina's NextSeq 2000 sequencing system (paired-end 2 x 151-bp, dual index 8-bp).

6-base-CUT&Tag (6B-C&T)

Preparation of tagmented DNA for 6-base sequencing

Feature-specific tagmentation was performed as in standard CUT&Tag, with modifications. Since the size selection and 6-base enzymatic conversion steps reduce DNA recovery, we increased input material to maintain DNA yields and PCR duplication rates comparable to conventional CUT&Tag. Four CUT&Tag samples (500,000 cells each) were prepared in parallel per biological sample. pA-Tn5-ME2U transposome was diluted 1:25 in dig-300 buffer and bound to cells for one hour at 25°C, followed by tagmentation. Proteinase K digestion was performed at 37°C for one hour and DNA was purified on Zymo DNA Clean and Concentrator. Eluted DNA from all four samples (i.e., 4 x 500,000 cells) was pooled and subjected to two rounds of right-side size selection (0.4X) with SPRI magnetic beads (Beckman Coulter) (*duet multiomics solution evoC* kit, biomodal) and Zymo column purification to remove untagmented genomic DNA. 4 pg of long DNA controls (tagmented unmethylated pUC19 and methylated Lambda DNA) were added to each sample at this stage. Gap repair was carried out with 8 U Phusion DNA polymerase (M0530S) and 320 U *Taq* DNA ligase (M0208S), in 1X *Taq* DNA ligase reaction buffer containing 0.8 mM dNTPs (NEB N0447S) at 37°C for one hour. DNA was purified on Zymo columns and digested in exonuclease digestion mix (1X NEB buffer 4 NEB B7004S, 40 U T7 Exonuclease NEB M0263S, 120 U RecJf NEB M0264S, 80 U Exonuclease I from *E. coli* NEB M0293S) for 4 hours at 37°C, followed by an additional round of Zymo column clean-up.

For optimisation of exonuclease digestion conditions, a range of enzymes were tested to specifically degrade linear dsDNA, in addition to the ones employed in the final workflow (see above). For tests with Exonuclease III (NEB M0206S), 1X rCutSMART (NEB B6004S) was used

as the reaction buffer along with 100 U of Exo III per 500,000-cell equivalent of CUT&Tag material. For tests with Exonuclease VIII-truncated (NEB M0545S), 10 U were used per 500,000-cell equivalent of CUT&Tag material, also in rCutSMART buffer.

6-base-seq library preparation

The following steps were performed with early access reagents from the *duet multiomics solution evoC* kit (biomodal). To digest ME2U hairpin termini, 23.7 µL of exonuclease-treated DNA (enriched for circular dumbbell-like fragments) were treated with 3 µL of HD enzyme (hairpin digestion module) and 3 µL HD buffer for 30 min at 37°C, followed by 1.8X SPRI clean-up (elution = 14 µL water). DNA was denatured at 95°C for 2 min and slowly cooled (-0.1°C/s) to 10°C to enable strand separation and hairpin re-folding. At this stage, 0.4 pg short hmC control oligonucleotide (spike-in) was added to the sample. Strand copy synthesis (SC module) was set up with 13 µL DNA, 2.5 µL SC buffer, 2 µL dNTP mix, 2 µL SC enzyme 1, 2 µL SC enzyme 2, 2.5 µL hmCP additive and 1 µL hmCP enzyme, incubated at 37°C for 30 min, followed by denaturation at 95°C for 2 min and slow cooling (-0.1°C/s) to 10°C. 2.5 µL fork-head adaptor were then added to the DNA sample, along with 0.5 µL hairpin ligation additive and 15 µL hairpin ligation mastermix, and the sample was incubated at 20°C for 15 min and cleaned up with 1.2X SPRI beads (elution = 15 µL water). After ligation, the methyltransferase (MT) module was used to methylate the copy strand at unprotected 5mCpG sites. DNA from the previous step was mixed with 11.6 µL MT buffer, 0.4 µL MT additive 1, 1 µL MT additive 2 and 13 µL freshly reconstituted MT enzyme, incubated at 23°C for one hour, then at 65°C for 15 min, and cleaned up with 1.2X SPRI beads (elution = 31 µL water). 30 µL MT-treated DNA were treated with oxidation (Ox) mix (10 µL Ox additive 1 solution, made by reconstituting solid Ox additive 1 in 400 µL Ox buffer; 1 µL DTT solution; 1 µL hmCP additive; 1 µL hmCP enzyme and 2 µL Ox enzyme), followed by addition of 1 µL of 1:1250 dilution of Ox additive 2. Samples were incubated at 37°C for one hour and cleaned up with 1.8X SPRI beads (elution = 31 µL water). Deamination (DA module) was performed on 30 µL DNA by adding 12.7 µL water, 17.5 µL DA buffer, 1.8 µL ATP, 3.5 µL $MgCl_2$, 2 µL DA enzyme 1 and 2.5 µL DA enzyme 2 and incubating at 37°C for 90 min. Samples were purified by adding 6.5 µL DA clean-up reagent and concentration with 1.2X SPRI beads (elution = 21 µL water). 20 µL DNA were then PCR-amplified with 25 µL PCR mastermix and 5 µL UDI primers (programme: 98°C 30s; 12 cycles of 98°C 10s, 62°C 30s, 65°C 60s; final extension at 65°C 5 min; 4°C hold). DNA was purified with 0.9X SPRI beads (elution = 14 µL *evoC* dilution buffer), analysed on a 4200 TapeStation and quantified with the NEBNext library quantification kit. Sequencing was performed on the NextSeq 2000 platform (paired-end 2 x 151-bp, dual index 8-bp).

6B-C&T workflow without gap repair and exonuclease digestion

We initially developed 6B-C&T using a strategy for end repair of hairpin-containing tagmented DNA which slightly differs from the final optimized workflow (Supplementary Figure 1). After two rounds of SPRI removal of untagmented material, DNA was end-repaired via strand displacement of the inserted hairpin and gaps were filled in using Phi29 DNA polymerase (NEB M0269S). The reaction (25 µL) was set up with SPRI-eluted DNA, 1X Phi29 DNA polymerase reaction buffer, 0.2 mM dNTPs, 0.3 U/µL Phi29 DNA Pol and 0.1 mg/mL albumin, and incubated at 30°C for 30 min, then 65°C for 10 min, followed by Zymo column clean-up. Eluted DNA was then subjected to USER treatment (HD enzyme from the *duet multiomics solution evoC* kit) to digest the original ME2U hairpin strands, followed by standard 6-base library construction.

Generation of ground-truth DNA methylation controls

For the 5hmC control, we used 80 bp oligonucleotides (ATDbio, UK)[26] that were either hydroxymethylated or unmodified at specific CpGs (Supplementary Data 1 – Table 2). Here, short synthetic oligonucleotides were first annealed in appropriate pairs and quantified using a dsDNA Qubit Quantification Assay kit (Qiagen). Then, 100 ng of the annealed oligonucleotide were ligated to synthetic ME2U hairpin adaptors. The construct was treated with USER enzyme and purified using SPRI beads.

For long genomic DNA controls, 40 ng of enzymatically methylated (methylated using a CpG methyltransferase) bacteriophage λ DNA (EpigenDX) were added to an equal proportion of unmethylated pUC19 isolated from a methylation-negative strain of Escherichia coli (Dam–, Dcm–), and quantified using a dsDNA Qubit Quantification Assay kit (Qiagen). This mixture was tagmented using Tn5 preloaded with the ME2U hairpin. The tagmented DNA was purified using SPRI beads.

Whole-genome 6-base-seq using Tn5 tagmentation

Sample preparation and genomic DNA isolation

E14TG2A cells were harvested, spun down and washed once with PBS + 0.1% BSA. After pelleting, the supernatant was removed and cells were stored at -20°C until genomic DNA extraction. Genomic DNA isolation was carried out using the Quick-DNA MicroPrep Kit (Zymo Research Cat No D3020) following manufacturer's instructions. Purified DNA was quantified using Qubit and stored at -20°C.

Tagmentation

To perform whole-genome Tn5-based 6-base-seq, the ME1U hairpin adaptor (Supplementary Data 1 – Table 2) was annealed in Nuclease-Free Duplex Buffer (30 mM HEPES, pH 7.5; 100 mM potassium acetate, IDT11-01-03-01) at 25 µM and then complexed in a 1:1 ratio with Tn5 in TPS buffer (Creative Enzymes Cat No NATE-1629). 12 pmol of loaded Tn5 were used to tagment 80 ng of genomic DNA. Tagmentation was carried out in LM Buffer (Creative Enzymes Cat No NATE-1629) for 10 min at 56°C. Before DNA purification, DNA was released by adding SDS to a final concentration of 0.05% and incubating at 55°C for 15 min. After incubation, DNA was purified with 1.8X SPRI beads and eluted in 16.5 µL of nuclease-free water. 1 µL of eluted DNA was analysed on a TapeStation to determine the tagmentation efficiency.

6-base-seq library prep and sequencing

15.5 µL tagmented DNA were first gap-filled with 8U of Phi29 DNA polymerase (NEB Cat No M0269) in Phi29 reaction buffer (1X Phi29 buffer, 200 µM dNTPs, 100 µg/ml albumin) by incubating at 30°C for 30 min, followed by denaturation at 65°C for 10 min. DNA was then purified with 0.9X SPRI beads and subjected to USER enzyme (NEB Cat No 5505) digestion (in 1X rCutSmart buffer, NEB B6004S) to cleave the original ME1U hairpin strand. After USER reaction, DNA was purified with 1.8X SPRI beads, eluted with 12 µL library dilution buffer (biomodal) and then denatured at 95°C for 2 min followed by slow cooling (0.1°C/s) to 10°C. Resulting DNA was processed using the *duet multiomics solution evoC* kit (biomodal) according to the protocol described for 6B-C&T and amplified with six PCR cycles. After PCR, samples were purified with 0.9X SPRI beads, eluted in dilution buffer (biomodal), quantified with Qubit and analysed by Tapestation. Sequencing was performed on a NovaSeq 6000 platform (paired-end 2 x 151-bp, dual index 8-bp).

Bioinformatic analysis and data visualisation

Standard CUT&Tag data analysis

Libraries were demultiplexed using *demuxFQ* (flags: -c -d -i -e -t 1 -r 0.01 -R -l 9). *FastQC*- version 0.11.8 was used to assess the read quality. Bases with a quality score below 20 were trimmed from both reads using *Cutadapt* (cutadapt -q 20). Reads were aligned to the mm10 reference genome using *bwa mem* with default parameters. Duplicates were removed using *Picard* version 2.20.3 (*Picard MarkDuplicates*). BigWig files were created on the deduplicated BAM file, using *deepTools bamCoverage* (parameters: *--normalizeUsing* CPM, *--binSize* 10). Peaks were called using *Seacr* version 1.3 without input control reporting the top 1% by AUC regions, using both relaxed and stringent criteria. For consensus peak calling, overlap across biological replicates was calculated with intervene tools generating a series of .bed files. Peaks that were common to at least 2 of the 3 biological replicates were considered as consensus peaks. Metagene profiles were generated using *deepTools*.

6-base sequencing data pre-processing

FASTQs from 6-base-seq libraries were processed through a modified version of biomodal's duet analysis pipeline. For 6B-C&T (ME2U hairpin), 9-nt scar sequences, AAGAGATAG (R1) and AAAAAACAA (R2), derived from the deaminated, USER-treated Tn5 mosaic end (ME) sequence, were trimmed from the 5' ends of reads 1 and 2, respectively. Read pairs that lacked either scar sequence were discarded. Adaptor sequences containing the full 19 nt Tn5 ME sequence and 2 uracils (ME2U) hairpin were trimmed from the 3' ends of reads 1 and 2. For whole-genome 6-base-seq (ME1U hairpin), NNNNNNNNAGATGTGTATAAGAGATAG (R1) & NNNNNNNNAAATATATATAAAAAACAA (R2) were trimmed from the 5' ends of reads 1 and 2, respectively. Similarly, read pairs that lacked either scar sequence were discarded. Adaptor sequences containing the full 19 nt Tn5 ME sequence and 1 uracil (ME1U) hairpin were trimmed from the 3' ends of reads 1 and 2.

In all cases, a further 9 bp were trimmed from the 3' ends of reads 1 and 2 to remove the gaps generated during Tn5 transposition. Trimmed read pairs were then resolved using the bespoke resolution algorithm from Füllgrabe et al[26]. The resolved, single-end reads were aligned against a GRCm38 reference (gencode vM25) that contained additional sequences for pUC19, bacteriophage lambda and short spike-in oligonucleotides using *bwa-mem2* (v2.2.1). Multimapping reads, secondary and supplementary alignments were filtered out. DNA (hydroxy)methylation was quantified per aligned position from MM tags as part of the duet analysis pipeline. Compiled sequencing data analysis reports for all datasets were obtained on NextFlow and are available in Supplementary Data 1 (Tables 3-7).

Call-rate matrix for 6B-C&T

A call-rate matrix was used (Figure 1g) to measure the accuracy of 5mC and 5hmC calls. Each cell in the matrix m represents the rate at which the method calls a particular modification state X when the true modification is Y. For example, the cell m(5mC, C) represents the rate at which the method calls unmodC when the true modification status is 5mC. Each row of the matrix corresponds to the rate at which each modification status is called for a particular true modification status. The matrix was estimated using three different spike-in controls: fully unmethylated pUC19 DNA for the row corresponding to a true state of unmethylated C; fully methylated lambda for the row corresponding to a true state of 5mC; and synthetic oligonucleotide for the row corresponding to a true state of 5hmC. For a given row, the rate is calculated as the proportion of bases with

each modification status in the set of bases for which the genetic base call is C and which are aligned to CpGs in the given control sequence.

Analysis and visualisation of 6B-C&T and WG 6B-seq data

Individual 5mC and 5hmC percentages were calculated at each CpG site for all replicates. For downstream analyses, only cytosines with a read coverage ≥ 20 were included, except for genome browser visualisation in IGV, where a minimum coverage of ≥ 10 was used. BigWig tracks for 6B-C&T–derived 5mC and 5hmC across the four histone marks were generated by merging individual replicates. Merged bedGraph files were created using bedtools (v2.31.0), and BigWig files for IGV visualisation were produced using bedGraphToBigWig.

Average 5mC and 5hmC percentages were calculated for each replicate of the 6B-C&T datasets (across the four histone marks) and the whole-genome 6-base-seq dataset using a custom R script. Differential methylation analyses, including generation of volcano plots, were performed for each 6B-C&T dataset relative to whole-genome 6-base-seq using methylKit (v1.34.0). Window-based analyses were conducted with the methylKit tiling function (win.size = 100; step.size = 100). Cytosines with read coverage < 20 were excluded during methylKit processing. Differentially methylated positions were identified using the *calculateDiffMeth* function. Regions with $p < 0.05$, $|\log2FC| \geq 0.5$, and an absolute methylation difference ≥ 15% between groups were defined as differentially methylated regions (DMRs).

Shared CpG enrichment profiles were generated using a custom bash workflow. The mm10 genome was partitioned into 1 kb bins, and average enrichment values for each histone mark were computed across these bins using standard CUT&Tag datasets. For CpGs shared between whole-genome 6-base-seq and 6B-C&T datasets, cytosine modification percentages were plotted as a function of histone mark enrichment ($\log_2$ scale) for each histone mark.

Average read profiles for 6B-C&T centred on each enhancer class were generated using deepTools. Briefly, bamCoverage was used to produce BigWig files from BAM files containing 6B-C&T–resolved reads, using a bin size of 20. Peak density distributions were computed with computeMatrix (100 bp bins) and visualised with plotProfile. The enhancer analysis for global distributions of 5mC and 5hmC was performed using a custom R script (v4.3.1). Briefly, all CpG sites overlapping with enhancer peaks (primed, poised, or active, defined in Cruz-Molina et al.[40]) were identified with *BEDTools* and levels of each CpG state (C, 5mC and 5hmC) at each enhancer were calculated and visualised using R and GraphPad Prism.

Publicly available CUT&Tag-BS data for mESCs were downloaded as raw FASTQ files from the European Nucleotide Archive (ENA), EMBL. Adapter sequences were removed using Cutadapt with the parameters "-a CTGTCTCTTATACAC -A CTGTCTCTTATACAC -O 5 -q 0 -m 20 -p". The trimmed reads were subsequently aligned to mm10 genome using Bismark v0.24.044[46] with parameters "-X 1000 --non_bs_mm". Publicly available ChIP-seq datasets for WT mESCs were downloaded from GEO. Raw reads were filtered to remove those with a mean base quality score <20 and aligned to the mouse genome (mm10) using BWA. The resulting BAM files were processed, and peak calling was performed with MACS2[47] with parameters $p \leq 0.01$; Fold-enrichment ≥ 2 and Broad Region Calling ON.

Distributions of 5mC and 5hmC levels across genomic windows (IGV snapshots) were visualized using a custom Python workflow that parsed TSV input files and removed invalid entries. Boxplots comparing methylation values across each enhancer mark and IgG were generated with matplotlib, using a fixed colour palette and ordering groups by their median values.

For differential methylation scatter plots, DSS-like estimates of mean CpG methylation for the two treatment groups (6B-C&T and WG 6B-seq), along with dispersion parameters, Wald statistics, and FDR-adjusted q-values, were derived from the *calculateDiffMeth* output of the methylkit package. These metrics were used to visualise concordance between treatment methylation means (μ_1 vs μ_2) by generating jittered, rasterized scatter plots using *ggplot2*.

Pearson correlations of modified CpG fractions between 6B-C&T and other libraries were computed for CpGs with ≥20× coverage. Pairwise correlations within samples were obtained using the *getCorrelation* function from the methylKit package.

Chemical structures in Figure 1a were generated using *ChemDraw*®. IGV[48] was used for data visualisation in Figure 1c, Figure 2b and Figure 3a. Plots in Figure 3b, Figure 3d, Supplementary Figure 4 and Supplementary Figure 16 were generated with Prism (GraphPad Software, Massachusetts USA).

Machine learning analysis

Data preparation

Raw counts were collected for each methylation state (C, 5mC, 5hmC and ambiguous modC, (i.e., modified C sites that cannot be resolved into 5mC or 5hmC) from 6-base-seq data (6B-C&T or WG 6B-seq). Raw counts were then normalised by the total CpG count (genome-wide), and then the average was taken across experimental replicates. CpG sites mapping to enhancer regions were collected, and the sequential CpG methylation states in each enhancer region were organised as a sample.

Model architecture

As H3K4me1 is the common feature of annotated active, poised, and primed enhancers, we used the samples curated from methylation profiles obtained from H3K4me1 6B-C&T to train a model for classification into these three enhancer classes. To further address the advantages of using H3K4me1-enriched 5mC and 5hmC information, we also trained an independent model with the same architecture based on the methylation profiles generated by whole genome 6B-seq. The model architecture (Supplementary Figure 17) consists of a linear projection layer that projects the normalised CpG methylation states to a 32-dimension vector (*d_model*). This projection layer was followed by a self-attention layer, which consisted of four attention heads (*num_head*) and a two-layer feed-forward network with 256 hidden units (*ff_dim*), and was used to extract the features for the final classification layer. The classification layer is a two-layer fully connected neural network with 256 hidden units (*mlp_h_dim*) for each layer. The 'elu' activation function was used for non-linearity. A dropout probability of 0.2 (*dropp*) was set for avoiding overfitting. CpG methylation profiles from chromosome 1 were retained for model evaluation.

Enhancer classification

Enhancer regions were defined and classified into three categories (active, poised, and primed) according to a previous study[40]. Here, we designed a machine learning model to predict the type of each enhancer based on its 6-base methylation profile. Specifically, for a set of enhancers $\mathbf{E} = \{\mathbf{e_1}, \mathbf{e_2}, \ldots, \mathbf{e_n}\}$, each enhancer can be represented as a sequential vector of normalized signals {*num_ambiguous_modC, mC, hmC, C*} for its CpG loci. Specifically, $\mathbf{e_i} = [\mathbf{m_1^i}, \mathbf{m_2^i}, \ldots, \mathbf{m_k^i}]$,

where m_j^i is the j-th CpG locus in the i-th enhancer, given by $\mathbf{m_j^i} = [x_{ambiguous\_modC}, x_{mC}, x_{hmC}, x_C]$, and x represents the normalized signal. The enhancer labels can be noted as $\mathbf{Y} \in \{0, 1, 2\}^n$, where 0 means active, 1 means poised, and 2 means primed. The classification task is then to find a classifier $f: \mathbf{e} \rightarrow \mathbf{y}$ to minimize the expected loss:

$$f^* = \text{argmin}_{f \in F} E[L(f(\mathbf{e}), \mathbf{y})]$$

Where $L(\cdot)$ is a loss function, we used the cross-entropy loss for the classification task.

Self-attention

To capture the associations among CpG methylation states in enhancers, we applied a self-attention module to the model[49]. After projection to a high-dimension space by the linear projector, the CpG methylation profile is simultaneously used as a query, key, and value matrix to calculate the attention matrix and the weighted value. The weighted value is then converted to informative embedding, which is further used for classification.

Statistics & reproducibility

Experiments were performed independently with different E14TG2A cultures (N = 2 for H3K27me3 6B-C&T; N = 3 for H3K27ac 6B-C&T; N = 3 for H3K4me1 6B-C&T; N = 3 for H3K4me3 6B-C&T; N = 3 for IgG 6B-C&T and N = 2 for WG 6B-seq) and no statistical method was used to predetermine sample size. Pearson correlation coefficient, representing effect size, was used to verify reproducibility. No data were excluded from any analyses. Descriptive statistics were computed using GraphPad Prism 10 (GraphPad) or R. Randomization or blinding were not required nor performed in this study. Differences between groups were assessed in Supplementary Figure 10 using *methylKit*, which employs a logistic regression test for p-value calculation, and in Supplementary Figure 14 using a Wilcoxon rank sum text (results in Supplementary Data 1 – Table 1).

Data availability

Sequencing data generated in this study is available through NCBI Gene Expression Omnibus under accession code GSE296587 [https://www.ncbi.nlm.nih.gov/geo/query/acc.cgi?acc=GSE296587], with no access restrictions. Publicly available mouse ESC CUT&Tag-BS data were obtained from GEO under accession code GSE179266 [https://www.ncbi.nlm.nih.gov/geo/query/acc.cgi?acc=GSE179266] and ChIP-seq datasets were obtained from GEO under accession code GSE89211 [https://www.ncbi.nlm.nih.gov/geo/query/acc.cgi?acc=GSE89211]. Source data are provided with this paper.

Code availability

Code is available on GitHub at https://github.com/sblab-informatics/6B-CUTnTag, with no access restrictions.

References

1. Bannister, A.J. & Kouzarides, T. Regulation of chromatin by histone modifications. *Cell Res* **21**, 381-95 (2011).
2. Zhong, Z. *et al.* DNA methylation-linked chromatin accessibility affects genomic architecture in Arabidopsis. *Proc Natl Acad Sci U S A* **118**(2021).
3. Sinha, K.K., Bilokapic, S., Du, Y., Malik, D. & Halic, M. Histone modifications regulate pioneer transcription factor cooperativity. *Nature* **619**, 378-384 (2023).
4. Yin, Y. *et al.* Impact of cytosine methylation on DNA binding specificities of human transcription factors. *Science* **356**(2017).
5. Bird, A. DNA methylation patterns and epigenetic memory. *Genes Dev* **16**, 6-21 (2002).
6. Law, J.A. & Jacobsen, S.E. Establishing, maintaining and modifying DNA methylation patterns in plants and animals. *Nat Rev Genet* **11**, 204-20 (2010).
7. Ito, S. *et al.* Role of Tet proteins in 5mC to 5hmC conversion, ES-cell self-renewal and inner cell mass specification. *Nature* **466**, 1129-33 (2010).
8. Ito, S. *et al.* Tet proteins can convert 5-methylcytosine to 5-formylcytosine and 5-carboxylcytosine. *Science* **333**, 1300-3 (2011).
9. Bachman, M. *et al.* 5-Hydroxymethylcytosine is a predominantly stable DNA modification. *Nat Chem* **6**, 1049-55 (2014).
10. Xu, Y. *et al.* Genome-wide regulation of 5hmC, 5mC, and gene expression by Tet1 hydroxylase in mouse embryonic stem cells. *Mol Cell* **42**, 451-64 (2011).
11. Ficz, G. *et al.* Dynamic regulation of 5-hydroxymethylcytosine in mouse ES cells and during differentiation. *Nature* **473**, 398-402 (2011).
12. Hon, G.C. *et al.* 5mC oxidation by Tet2 modulates enhancer activity and timing of transcriptome reprogramming during differentiation. *Mol Cell* **56**, 286-297 (2014).
13. Kozlenkov, A. *et al.* A unique role for DNA (hydroxy)methylation in epigenetic regulation of human inhibitory neurons. *Sci Adv* **4**, eaau6190 (2018).
14. Wu, F. *et al.* Spurious transcription causing innate immune responses is prevented by 5-hydroxymethylcytosine. *Nat Genet* **55**, 100-111 (2023).
15. Schubeler, D. Function and information content of DNA methylation. *Nature* **517**, 321-6 (2015).
16. Kreibich, E. & Krebs, A.R. Relevance of DNA methylation at enhancers for the acquisition of cell identities. *FEBS Lett* **597**, 1805-1817 (2023).
17. Szulwach, K.E. *et al.* Integrating 5-hydroxymethylcytosine into the epigenomic landscape of human embryonic stem cells. *PLoS Genet* **7**, e1002154 (2011).
18. Mellen, M., Ayata, P., Dewell, S., Kriaucionis, S. & Heintz, N. MeCP2 binds to 5hmC enriched within active genes and accessible chromatin in the nervous system. *Cell* **151**, 1417-30 (2012).
19. Clark, S.J., Harrison, J., Paul, C.L. & Frommer, M. High sensitivity mapping of methylated cytosines. *Nucleic Acids Res* **22**, 2990-7 (1994).
20. Booth, M.J. *et al.* Quantitative sequencing of 5-methylcytosine and 5-hydroxymethylcytosine at single-base resolution. *Science* **336**, 934-7 (2012).
21. Yu, M. *et al.* Base-resolution analysis of 5-hydroxymethylcytosine in the mammalian genome. *Cell* **149**, 1368-80 (2012).
22. Schutsky, E.K. *et al.* Nondestructive, base-resolution sequencing of 5-hydroxymethylcytosine using a DNA deaminase. *Nat Biotechnol* (2018).

23. Liu, Y. *et al.* Bisulfite-free direct detection of 5-methylcytosine and 5-hydroxymethylcytosine at base resolution. *Nat Biotechnol* **37**, 424-429 (2019).
24. Liu, Y. *et al.* Subtraction-free and bisulfite-free specific sequencing of 5-methylcytosine and its oxidized derivatives at base resolution. *Nat Commun* **12**, 618 (2021).
25. Searle, B., Muller, M., Carell, T. & Kellett, A. Third-Generation Sequencing of Epigenetic DNA. *Angew Chem Int Ed Engl* **62**, e202215704 (2023).
26. Fullgrabe, J. *et al.* Simultaneous sequencing of genetic and epigenetic bases in DNA. *Nat Biotechnol* **41**, 1457-1464 (2023).
27. Viswanathan, R. *et al.* DARESOME enables concurrent profiling of multiple DNA modifications with restriction enzymes in single cells and cell-free DNA. *Sci Adv* **9**, eadi0197 (2023).
28. Bai, D. & Zhu, C. SIMPLE-seq to decode DNA methylation dynamics in single cells. *Nat Rev Genet* **25**, 377 (2024).
29. Brinkman, A.B. *et al.* Sequential ChIP-bisulfite sequencing enables direct genome-scale investigation of chromatin and DNA methylation cross-talk. *Genome Res* **22**, 1128-38 (2012).
30. Statham, A.L. *et al.* Bisulfite sequencing of chromatin immunoprecipitated DNA (BisChIP-seq) directly informs methylation status of histone-modified DNA. *Genome Res* **22**, 1120-7 (2012).
31. Feldmann, A. *et al.* Transcription factor occupancy can mediate active turnover of DNA methylation at regulatory regions. *PLoS Genet* **9**, e1003994 (2013).
32. Li, R., Grimm, S.A. & Wade, P.A. CUT&Tag-BS for simultaneous profiling of histone modification and DNA methylation with high efficiency and low cost. *Cell Rep Methods* **1**(2021).
33. Grunau, C., Clark, S.J. & Rosenthal, A. Bisulfite genomic sequencing: systematic investigation of critical experimental parameters. *Nucleic Acids Res* **29**, E65-5 (2001).
34. Huang, Y. *et al.* The behaviour of 5-hydroxymethylcytosine in bisulfite sequencing. *PLoS One* **5**, e8888 (2010).
35. Pham, T.T. *et al.* Single-locus enrichment without amplification for sequencing and direct detection of epigenetic modifications. *Mol Genet Genomics* **291**, 1491-504 (2016).
36. Nanda, A.S. *et al.* Direct transposition of native DNA for sensitive multimodal single-molecule sequencing. *Nat Genet* **56**, 1300-1309 (2024).
37. Andersson, R., Sandelin, A. & Danko, C.G. A unified architecture of transcriptional regulatory elements. *Trends Genet* **31**, 426-33 (2015).
38. Habibi, E. *et al.* Whole-genome bisulfite sequencing of two distinct interconvertible DNA methylomes of mouse embryonic stem cells. *Cell Stem Cell* **13**, 360-9 (2013).
39. Acurzio, B. *et al.* Zfp57 inactivation illustrates the role of ICR methylation in imprinted gene expression during neural differentiation of mouse ESCs. *Sci Rep* **11**, 13802 (2021).
40. Cruz-Molina, S. *et al.* PRC2 Facilitates the Regulatory Topology Required for Poised Enhancer Function during Pluripotent Stem Cell Differentiation. *Cell Stem Cell* **20**, 689-705 e9 (2017).
41. Alajem, A. *et al.* DNA methylation patterns expose variations in enhancer-chromatin modifications during embryonic stem cell differentiation. *PLoS Genet* **17**, e1009498 (2021).

42. Geisenberger, C. *et al.* Single-cell multi-omic detection of DNA methylation and histone modifications reconstructs the dynamics of epigenomic maintenance. *Nat Methods* **22**, 2042-2051 (2025).
43. Hui, W.W.I., Simeone, A., Zyner, K.G., Tannahill, D. & Balasubramanian, S. Single-cell mapping of DNA G-quadruplex structures in human cancer cells. *Sci Rep* **11**, 23641 (2021).
44. Kaya-Okur, H.S. *et al.* CUT&Tag for efficient epigenomic profiling of small samples and single cells. *Nat Commun* **10**, 1930 (2019).
45. Fujiwara, Y. *et al.* Preparation of optimized concanavalin A-conjugated Dynabeads(R) magnetic beads for CUT&Tag. *PLoS One* **16**, e0259846 (2021).
46. Krueger, F. & Andrews, S.R. Bismark: a flexible aligner and methylation caller for Bisulfite-Seq applications. *Bioinformatics* **27**, 1571-2 (2011).
47. Zhang, Y. *et al.* Model-based analysis of ChIP-Seq (MACS). *Genome Biol* **9**, R137 (2008).
48. Robinson, J.T. *et al.* Integrative genomics viewer. *Nat Biotechnol* **29**, 24-6 (2011).
49. Vaswani, A. *et al.* Attention Is All You Need. *Advances in Neural Information Processing Systems 30 (Nips 2017)* **30**(2017).

Acknowledgements

We thank staff from the Research Instrumentation and Cell Services and the Genomics core facilities at the Cancer Research UK Cambridge Institute for research support. We thank previous and former members of the Balasubramanian group for helpful discussions on the development and application of 6B-C&T, especially Alice Dubois-Veltman, Zutao Yu, Sean M Flynn and Larry Melidis. The Balasubramanian laboratory is supported by CRUK core funding (C9681/A29214 to S.B.), CRUK programme funding (C9681/A29214 to S.B.) and University of Cambridge Herchel Smith funds (S.B.). S.B. is a Senior Investigator of the Wellcome Trust (209441/Z/17/Z).

Author contributions

R.C.A.T., D.T. and S.B. conceived the study. R.C.A.T. led the study, developed and optimised the 6B-C&T workflow, with wet-lab and computational input from S.D., J.M., M.T., P.G., A.C-U. and W.G. S.D. performed bioinformatic analyses with input from J.M. X.H. performed the machine learning analysis. All authors contributed to interpreting the results and provided critical feedback. R.C.A.T. created the figures with input from S.D., X.H. and J.M. R.C.A.T., D.T. and S.B. wrote the manuscript with contributions from all authors.

Competing interests

S.B. is a founder and shareholder of biomodal Ltd, GenomeTx and RNAvate Ltd and a science partner and paid adviser to Ahren Innovation Capital LLC. J.M., M.T., P.G., A.C-U. and W.G. are employees of biomodal Ltd. The remaining authors declare no competing interests.

Figure legends

Figure 1. 6-base-CUT&Tag conceptualisation. (a) Scheme depicting cytosine (C) methylation by DNA methyltransferase (DNMT) to form 5mC and progressive oxidation by (Ten-Eleven Translocation) TET enzymes to generate 5hmC, 5fC and 5caC modifications. Both 5fC and 5caC can be excised by thymine DNA glycosylase (TDG) to restore C and complete the demethylation cycle. Chemical groups specific to each cytosine state are flagged in red. **(b)** Conceptual overview

illustrating how 'standard' whole-genome 6-base sequencing reports an average ensemble picture that does not accurately represent co-occurring epigenetic features. In contrast, enriching for a specific chromatin feature (e.g., H3K27ac mark) isolates a sub-family of co-occurring protein-DNA fragments and simultaneously reports on 5mC and 5hmC at read level. For simplicity, methylation heterogeneity for each modification is not represented in this scheme. Schematic 5mC and 5hmC percentages are shown for the CpG sites in each case. **(c)** Complete 6-base-CUT&Tag (6B-C&T) workflow. Specific steps are detailed in the main text (also see Supplementary Figure 1). An example profile for H3K27ac, 5mC and 5hmC is shown at the bottom of the diagram and exemplifies the coupling of three layers of information originating from the same DNA fragment. Colour code for selected nucleobases is indicated throughout the diagram.

Figure 2. 6-base-CUT&Tag implementation and benchmarking. (a) Left: strategy to enrich *bona fide* 6B-C&T fragments. In this workflow, exonuclease enzymes are first used to digest randomly cleaved or partially tagmented DNA to enrich circularised DNA containing hairpins on both ends. USER digestion is then used to open circular fragments and separate each strand, allowing for hairpin re-folding followed by subsequent copy strand synthesis and ligation of fork-head adaptors. Ligated DNA is now ready for 6-base-seq enzymatic conversions and PCR amplification. After paired-end sequencing, the presence of USER-derived scar sequences on both R1 and R2 reads identifies valid 6-base-seq fragments. Right: percentage of USER-scarred paired-end reads for different exonuclease cocktails tested after gap filling and nick sealing. The protocol without these steps (black) is shown as a control (Methods). Data from H3K27ac profiling in E14TG2A mESCs. **(b)** Representative genome browser view of 6-base-H3K27ac-CUT&Tag (green) and standard H3K27ac-CUT&Tag (blue) profiles (coordinates shown under the tracks). **(c)** Metagene plot showing H3K27ac enrichment for 6B-C&T data in peak regions defined using standard H3K27ac-CUT&Tag data. CPM-normalized CUT&Tag coverage is plotted relative to the centre of each consensus peak. **(d)** Call-rate matrix for 5mC and 5hmC detection in three fiducial DNA controls used in 6B-C&T. Rows represent the true modification state of individual cytosines in each control (C – pUC19 unmethylated DNA; 5hmC – synthetic modified oligonucleotide; 5mC – fully methylated lambda DNA), while columns indicate the experimentally called modification state (calls). Numbers represent the % calls for each column category in each row type. Source data are provided as a Source Data file.

Figure 3. Histone mark-specific 5mC and 5hmC signatures define different mESC enhancer states. (a) Genome browser views of representative active, primed and poised enhancer loci. Tracks show histone mark levels and percentages of 5mC and 5hmC obtained with 6B-C&T for enhancer-associated histone marks, in addition to IgG control. The genomic location of each annotated enhancer is indicated with a horizonal bar and shaded area coloured according to enhancer type (active – blue, primed – green and poised – red). Tracks within each group (CUT&Tag fragment enrichments, %5mC and %5hmC) have the same y-axis scale. **(b)** Stacked bar plots showing average (mean) relative percentages of CpG methylation states for each enhancer type at different associated histone marks (data from biologically independent replicates: H3K27me3, N = 2; H3K27ac, N = 3; H3K4me1, N = 3). Error bars show standard deviation. The top bar graph shows the total distribution of detected unmodified C, 5mC and 5hmC, while the bottom graph shows the relative abundances of 5mC and 5hmC. **(c)** Normalized 6B-C&T read coverages in primed enhancer regions for H3K27ac, H3K4me1 and H3K27me3. Data from one representative experiment plotted relative to the centre of each enhancer region. Replicate information as in **b**. **(d)** Stacked bar plots of mean CpG methylation percentages for each histone modification at primed enhancers. Left: all 6-base-seq CpG states (C, 5mC and 5hmC). Right: quantification of the relative abundances of 5mC and 5hmC at each histone mark across biologically independent replicates (H3K27me3, N = 2; H3K4me1, N = 3; H3K27ac, N = 3). Error bars represent standard deviation. Source data are provided as a Source Data file.

Figure 4. H3K4me1-specific 5mC and 5hmC levels are robust predictors of mESC functional enhancer states. (a) Machine learning workflow for enhancer type classification using 6B-C&T (H3K4me1) and whole genome (WG) 6B-seq data. Read-level 5mC and 5hmC counts are extracted from each dataset (see Methods) and used together with reference enhancer annotations (labels) to train a classification model to resolve different enhancer types (samples). Enhancer annotations were obtained from Cruz-Molina et al.[40] **(b)** Performance evaluation for H3K4me1 6B-C&T-based vs. whole genome 6B-seq-based models. Precision-recall and Receiver Operating Characteristic curves are shown for each model using chromosome 1 data as a test set (not included in training). **(c)** Multi-class precision-recall curves for different training vs. test dataset combinations (e.g., WG on 6B-C&T: trained on whole genome data and tested on 6B-C&T data). All tests were performed on chromosome 1 data (not included in training) using the trained model for classification into different enhancer types. **(d)** Multi-class Receiver Operating Characteristic curves for the machine learning routine described in **c**. Colour legend and area under the curve (AUC) values are shown below each graph. Source data are provided as a Source Data file.

Editor's Summary

Chemical modifications on DNA are key regulators of epigenetic function. Here, the authors develop 6-base-CUT&Tag to simultaneously profile multiple DNA and chromatin features on the same DNA fragment. This work reveals how specific DNA and histone marks colocalise at different enhancer regions.

Peer Review Information: *Nature Communications* thanks the anonymous reviewer(s) for their contribution to the peer review of this work. A peer review file is available.

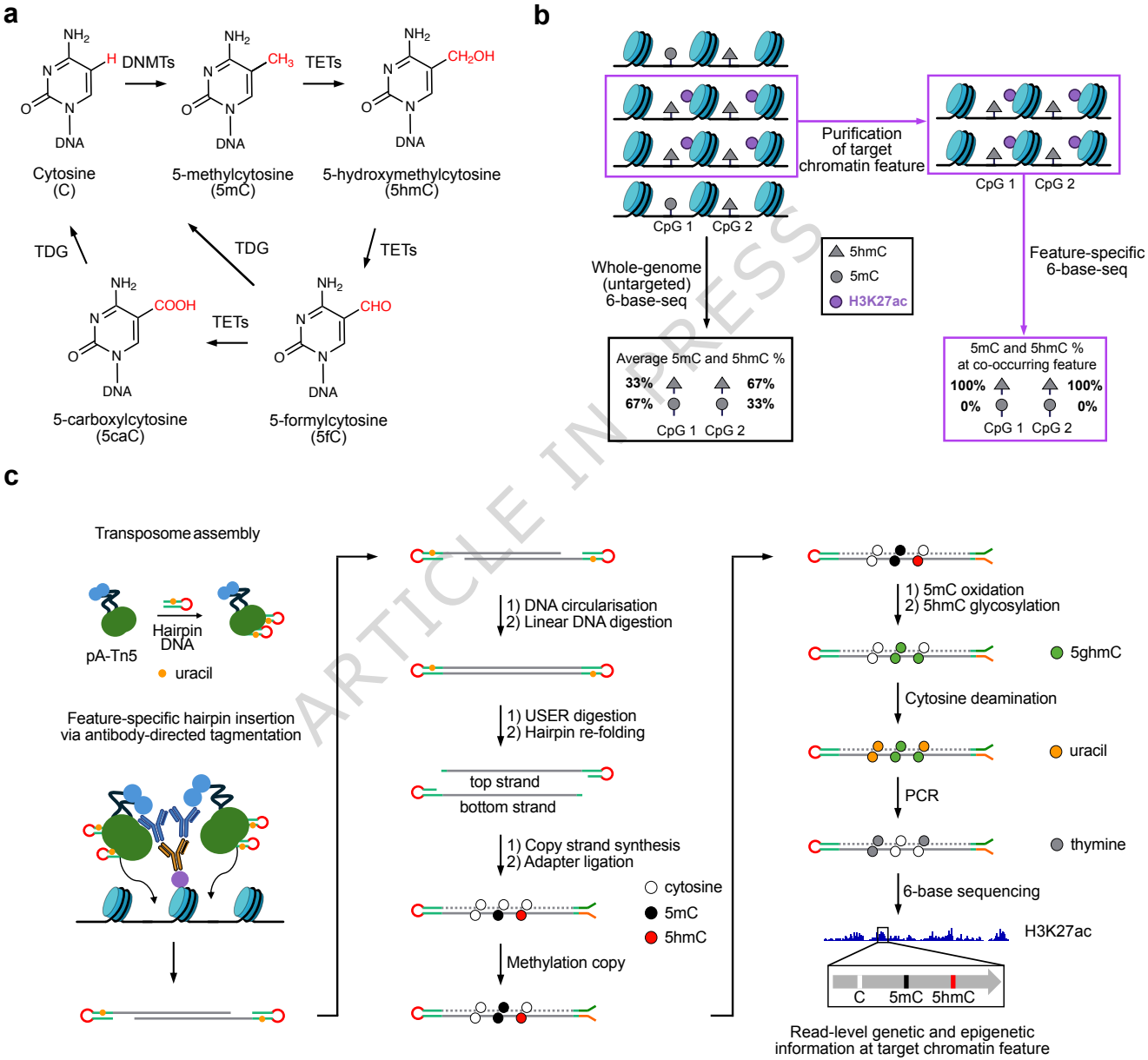

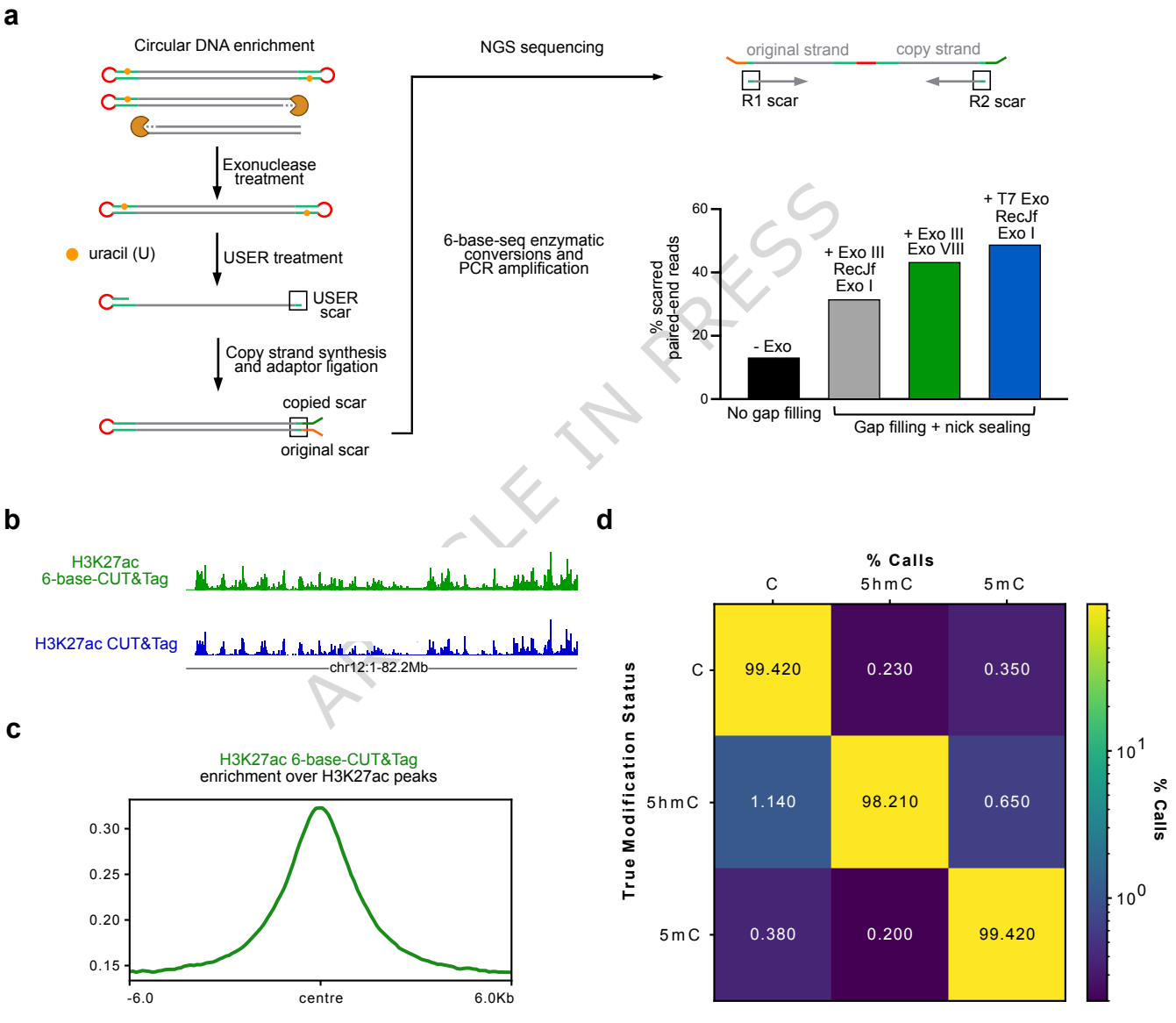

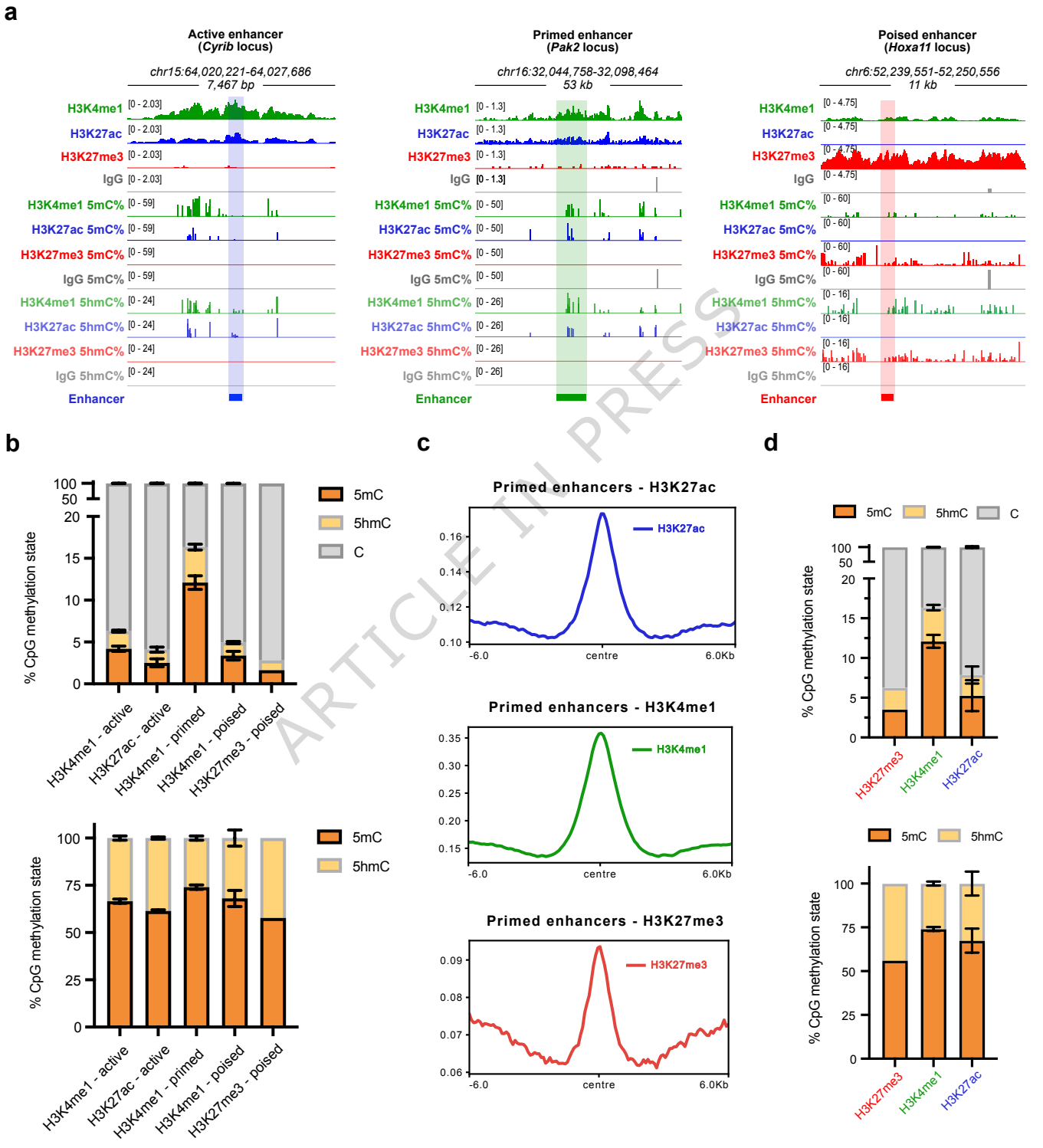

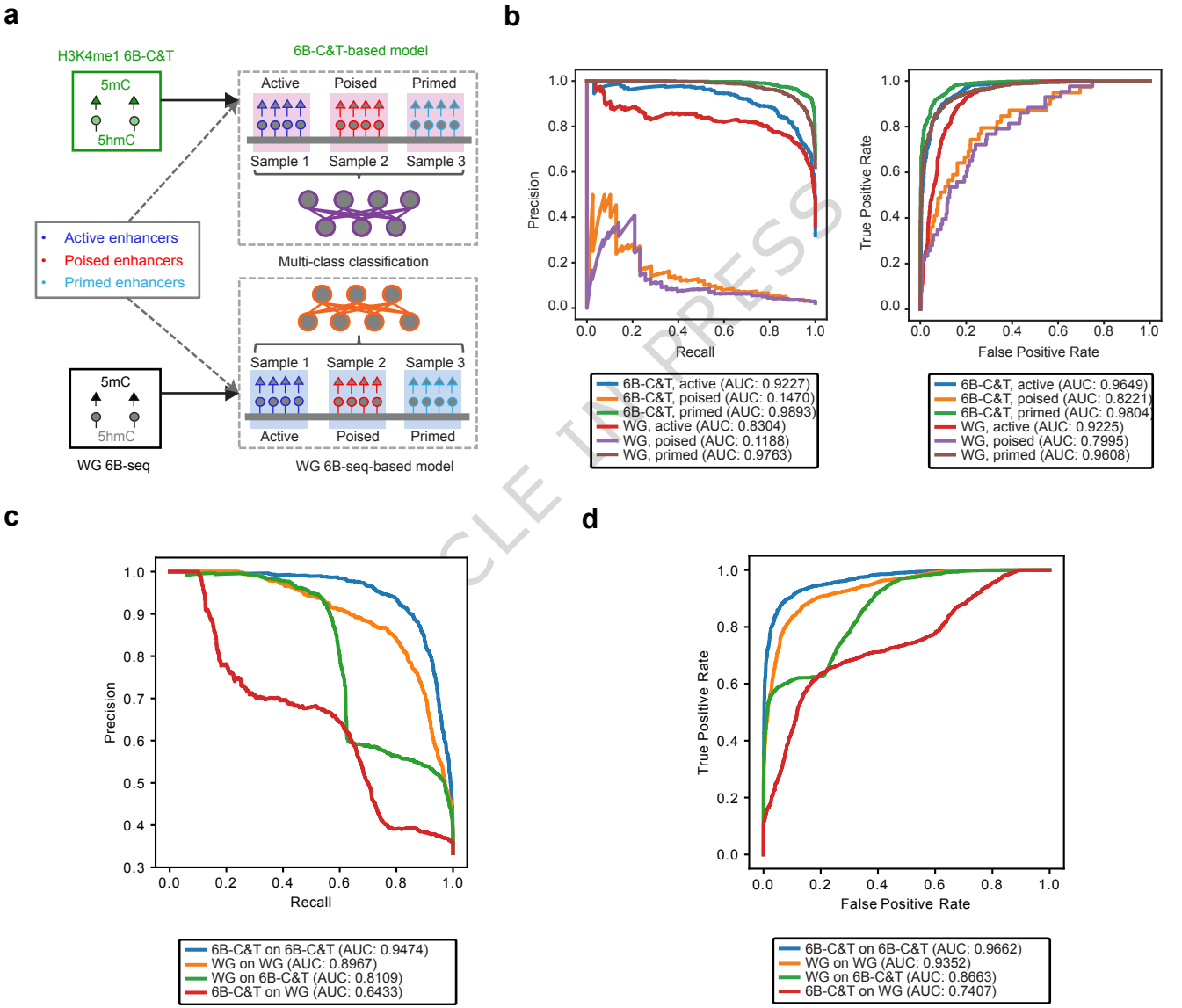
a
H3K4me1 6B-C&T
5mC
5hmC
6B-C&T-based model
Active
Poised
Primed
Sample 1
Sample 2
Sample 3
Active enhancers
Poised enhancers
Primed enhancers
Multi-class classification
5mC
5hmC
WG 6B-seq
WG 6B-seq-based model
b
Precision
Recall
6B-C&T, active (AUC: 0.9227)
6B-C&T, poised (AUC: 0.1470)
6B-C&T, primed (AUC: 0.9893)
WG, active (AUC: 0.8304)
WG, poised (AUC: 0.1188)
WG, primed (AUC: 0.9763)
True Positive Rate
False Positive Rate
6B-C&T, active (AUC: 0.9649)
6B-C&T, poised (AUC: 0.8221)
6B-C&T, primed (AUC: 0.9804)
WG, active (AUC: 0.9225)
WG, poised (AUC: 0.7995)
WG, primed (AUC: 0.9608)
c
Precision
Recall
6B-C&T on 6B-C&T (AUC: 0.9474)
WG on WG (AUC: 0.8967)
WG on 6B-C&T (AUC: 0.8109)
6B-C&T on WG (AUC: 0.6433)
d
True Positive Rate
False Positive Rate
6B-C&T on 6B-C&T (AUC: 0.9662)
WG on WG (AUC: 0.9352)
WG on 6B-C&T (AUC: 0.8663)
6B-C&T on WG (AUC: 0.7407)